



Contents lists available at ScienceDirect

Journal of King Saud University – Science

journal homepage: [www.sciencedirect.com](http://www.sciencedirect.com)

# Removal of Pb(II) from aqueous solution using KCC-1: Optimization by response surface methodology (RSM)

R. Hasan<sup>a</sup>, H.D. Setiabudi<sup>a,b,\*</sup><sup>a</sup> Faculty of Chemical and Natural Resources Engineering, Universiti Malaysia Pahang, 26300 Gambang, Kuantan, Pahang, Malaysia<sup>b</sup> Centre of Excellence for Advanced Research in Fluid Flow, Universiti Malaysia Pahang, 26300 Gambang, Kuantan, Pahang, Malaysia

## ARTICLE INFO

### Article history:

Received 25 July 2018

Accepted 15 October 2018

Available online 17 October 2018

### Keywords:

KCC-1

Pb(II) removal

Adsorption

Optimization

Response surface methodology

## ABSTRACT

The performance of KCC-1 as adsorbent towards Pb(II) removal was investigated. The TEM, XRD, FTIR, and BET results proved that the synthesized KCC-1 contains fibrous silica structure with the surface area of 298.87 m<sup>2</sup>/g. The influence of prominent factors (initial concentration ( $X_1$ ), time ( $X_2$ ) and adsorbent dosage ( $X_3$ )) on Pb(II) removal was evaluated by response surface methodology (RSM). The most significant factor was the linear function of adsorbent dosage ( $X_3$ ), while the quadratic effect of time ( $X_2^2$ ) was the least significant factor. Maximum Pb(II) removal of 84.54% predictably and 83.06% experimentally were achieved under the optimal conditions ( $X_1 = 281.7$  mg/L,  $X_2 = 80$  min and  $X_3 = 3.7$  g/L). The feasibility of KCC-1 in Pb(II) removal was confirmed by its good performance during five cycles of reusability study. It is affirmed that the KCC-1 has a high potential to be used in adsorption of Pb(II) from aqueous solution. © 2018 The Authors. Production and hosting by Elsevier B.V. on behalf of King Saud University. This is an open access article under the CC BY-NC-ND license (<http://creativecommons.org/licenses/by-nc-nd/4.0/>).

## 1. Introduction

Wastewater effluent from various industries including mining, battery, metallurgical, and paints, contains a potentially dangerous amount of heavy metals for example lead, cadmium, mercury, and arsenic (Fatimah, 2018; Siddiqui, 2015; Yousefzadeh et al., 2018). Lead (Pb(II)) has been acknowledged as one of the most hazardous heavy metals, which may cause numerous health problems including damage to kidney, liver and nervous system (Ekka et al., 2015; Gang et al., 2015; Liu et al., 2011; Tan et al., 2012; Yousefzadeh et al., 2018). Additionally, Pb(II) is considered toxic even at low concentration (Rengaraj et al., 2001), with the permissible limit in drinking water of 0.015 mg/L and 0.01 mg/L, as set up by the United States Environmental Protection Agency (EPA, 2009) and World Health Organization (1984), respectively. Thus, Pb(II)-containing effluent must be properly treated before being discharged into receiving waters.

Numerous techniques have been reported for Pb(II) removal such as an exchange of ions (Rengaraj et al., 2001), coagulation-flocculation (Hargreaves et al., 2018), chemical precipitation (Merganpour et al., 2015), solvent extraction (Baba and Adekola, 2013) and adsorption (Ekka et al., 2015; Gomes et al., 2013; Radi et al., 2015). Among the stated techniques, adsorption process appears as an attractive method owing to its excellent removal capability, convenience, economic cost, and simplicity (Lalchhingpui et al., 2017; Lowe et al., 2015; Okoye et al., 2018; Tan et al., 2012). Mesoporous silica has attracted considerable attention for Pb(II) removal owing to its high surface area, good structural stability, accessible adsorption sites, and large uniform pores (Ekka et al., 2015; Lalchhingpui et al., 2017). Besides, the negative charge of the silica surface induce more active sites on the mesoporous material, thus enhance the adsorption process (Lowe et al., 2015).

Recently, a new type of mesoporous silica material which is known as fibrous silica nanosphere (KCC-1), has attracted much attention in various types of application such as hydrogen storage (Ouyang et al., 2016), catalysis (Siddiqui et al., 2014), and CO<sub>2</sub> capture-conversion (Hamid et al., 2017), due to its high surface area, fibrous surface morphology, wide pore diameter, high mechanical, and thermal stability (Borah et al., 2015; Polshettiwar et al., 2010; Qureshi et al., 2016). Owing to its excellent properties and performances, the application of KCC-1 as an adsorbent is promising to be explored. Additionally, there is no study on the application of KCC-1 towards the heavy metal

\* Corresponding author at: Faculty of Chemical and Natural Resources Engineering, Universiti Malaysia Pahang, 26300 Gambang, Kuantan, Pahang, Malaysia.

E-mail address: [herma@ump.edu.my](mailto:herma@ump.edu.my) (H.D. Setiabudi).

Peer review under responsibility of King Saud University.



Production and hosting by Elsevier

removal. It is expected that the fibrous morphology of KCC-1 will enhance the accessibility of active sites and consequently improve its performance on adsorption process. In this study, the optimal conditions of Pb(II) removal onto KCC-1 were investigated using Response Surface Methodology (RSM) combined with face-centered central design (FCCCD).

## 2. Materials and methods

### 2.1. Preparation of KCC-1

KCC-1 was prepared in accordance with a method described by Le et al. (2015) with minor modification. In brief, tetraethyl orthosilicate (2.6 g, Merck), butanol (1.5 mL, Merck), and toluene (30 mL, Merck) were stirred in one beaker (30 min, 30 °C), whereas urea (0.6 g, Merck), cetyltrimmonium bromide (CTAB, 1 g, Aldrich), and water (30 min, 30 °C) were stirred in another beaker (30 min). Both solutions were stirred in separate beaker to make sure the solutions are homogenous owing to the fact that the preparation of KCC-1 involves the microemulsion formation which required a highly homogeneous solution. Then, both solutions were mixed, stirred (45 min, 30 °C), and heated in a Teflon-sealed hydrothermal reactor (5 h, 120 °C). The obtained solution was centrifuged, rinsed, oven-dried (12 h, 100 °C), and calcined (5 h, 550 °C).

### 2.2. Characterization of KCC-1

The morphology of KCC-1 was imaged using transmission electron microscopy (TEM, Philips CM12), while the textural properties of KCC-1 were examined using Brunauer-Emmett-Teller (BET, Micromeritics®). The crystallinity texture of KCC-1 was examined via X-ray diffraction (XRD) recorded using powder diffractometer (Miniflex II, Rigaku; 30 kV, 15 mA) within the range of  $2\theta = 5^\circ\text{--}80^\circ$  with a Cu K $\alpha$  radiation ( $\lambda = 1.54 \text{ \AA}$ ). The functional groups participated in adsorption process were determined using Fourier-transform infrared spectrometer (FTIR, Nicolet iS5, Thermo Scientific).

### 2.3. Batch adsorption

The adsorption experiments were executed according to the experimental design generated from RSM. Prior to the analysis, the stock solution (100 mg/L) was prepared by dissolving an accurate quantity of Pb(II) nitrate ( $\text{Pb}(\text{NO}_3)_2$ , Sigma-Aldrich) in deionized water, before being diluted to the desired concentration. The initial pH of Pb(II) solution was adjusted using sodium hydroxide (NaOH, Merck) or hydrochloric acid (HCl, Merck) solution. Then, a specific amount of KCC-1 was added to the Pb(II) solution under constant stirring (30 °C). The samples from the adsorption experiments were collected at the specific time, followed by centrifugation (3000 rpm, 2 min). The residuals of the Pb(II) concentration were analysed using UV-vis spectroscopy at 520 nm. Dithizone was used as a reagent to give the brick red colour to the solution. The values of Pb(II) removed (%) and Pb(II) adsorbed (mg/g) were determined using the following equations:

$$\text{Removal (\%)} = \left( \frac{C_0 - C_t}{C_0} \right) \times 100 \quad (1)$$

$$q_t = \left( \frac{C_0 - C_t}{m} \right) \times V \quad (2)$$

where  $C_0$  and  $C_t$  (mg/L) is the concentration of Pb(II) solution at zero time and at any time, respectively.  $V$  (L) is the volume of the Pb(II) solution and  $m$  (g) is the mass of KCC-1 used.

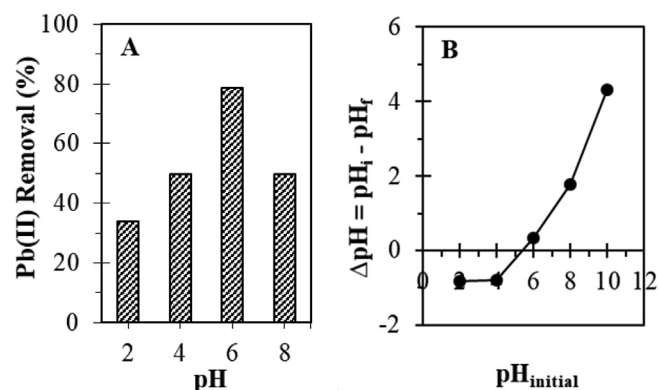


Fig. 1. (A) Influence of pH on Pb(II) removal by KCC-1 ( $C_0 = 200 \text{ mg/L}$ ,  $m_{\text{KCC-1}} = 4 \text{ g/L}$ ,  $T = 30^\circ\text{C}$ ,  $t = 80 \text{ min}$ ). (B)  $\text{pH}_{\text{zpc}}$  of the KCC-1.

In this study, the initial pH of Pb(II) solution was fixed at 6 according to the result obtained from the effect of pH as shown in Fig. 1(A). Additionally, the trend observed in Fig. 1(A) can be described on the basis of zero point charge ( $\text{pH}_{\text{zpc}}$ ) of KCC-1, which confirmed to be at  $\sim\text{pH}5.8$ , as shown in Fig. 1(B). Thus, Pb(II) adsorption was preferably occurred at pH value higher than  $\text{pH}_{\text{zpc}}$  owing to the electropositive property of Pb(II) ions. However, low Pb(II) removal was observed at pH 8 (Fig. 1(A)) might be due to the precipitation of Pb(II) in the form of hydroxide.

### 2.4. Experimental design and optimization

The FCCCD (Statsoft Statistica 8.0 software) was employed with three independent factors, namely initial concentration ( $X_1$ ), time ( $X_2$ ), and adsorbent dosage ( $X_3$ ). The design of experiments and corresponding results of response are accessible in Table 1. Each adsorption experiment was conducted triplicates for accuracy. The optimum condition of Pb(II) removal onto KCC-1 was predicted using the quadratic model obtained from the design. Evaluation of the applicability and the significance of the quadratic model was examined using analysis of variance (ANOVA).

## 3. Results and discussion

### 3.1. Characterization of KCC-1

The TEM images of KCC-1 with different magnifications are shown in Fig. 2. As illustrated in Fig. 2, the KCC-1 has uniform spheres with fibrous morphology, which expected will provide a high possibility of Pb(II) molecules to be trapped and thus can enhance the Pb(II) adsorption process. The XRD pattern of KCC-1 (Fig. 3(A)) showed a peak at  $2\theta \approx 23^\circ$ , corresponded to the amorphous silica (Le et al., 2015). Meanwhile, the FTIR spectrum of KCC-1 (Fig. 3(B)) showed the existent of several major peaks approximately at 3399, 1063, 799 and 448  $\text{cm}^{-1}$ , corresponded to the O-H stretching vibration mode of Si-OH, symmetrical stretching of Si-O, unsymmetrical stretching of Si-O and the bending of Si-O, respectively (Kelechi et al., 2018). The presence of silanol groups in KCC-1 is beneficial for adsorption process as the presence of negative charge results to a higher amount of available actives sites for adsorption process (Lowe et al., 2015). The  $\text{N}_2$  physisorption analysis showed that the pore volume ( $V_p$ ) and surface area ( $S_{\text{BET}}$ ) of synthesized KCC-1 was 0.3569  $\text{m}^3/\text{g}$  and 298.87  $\text{m}^2/\text{g}$ , respectively. High surface area of KCC-1 will improve the accessibility of Pb(II) molecules to the KCC-1 and thus enhance the adsorption process. The physical and chemical properties of the synthesized KCC-1 were comparable with the literatures (Ouyang

**Table 1**  
Design of experiments and experimental response for Pb(II) removal by KCC-1.

Run	Manipulated Variables						Response Pb(II) Removal, Y (%)
	Initial Concentration, $X_1$ (mg/L)		Time, $X_2$ (min)		Adsorbent Dosage, $X_3$ (g/L)		
	Coded	Uncoded	Coded	Uncoded	Coded	Uncoded	
1	-1	50	-1	60	-1	0.5	21.73
2	-1	50	-1	60	1	5	58.30
3	-1	50	1	140	-1	0.5	42.25
4	-1	50	1	140	1	5	78.14
5	1	400	-1	60	-1	0.5	51.00
6	1	400	-1	60	1	5	83.73
7	1	400	1	140	-1	0.5	67.86
8	1	400	1	140	1	5	68.14
9	-1	50	0	100	0	2.75	70.35
10	1	400	0	100	0	2.75	70.39
11	0	225	-1	60	0	2.75	80.93
12	0	225	1	140	0	2.75	84.77
13	0	225	0	100	-1	0.5	65.96
14	0	225	0	100	1	5	70.75
15(C)	0	225	0	100	0	2.75	83.67
16(C)	0	225	0	100	0	2.75	82.58

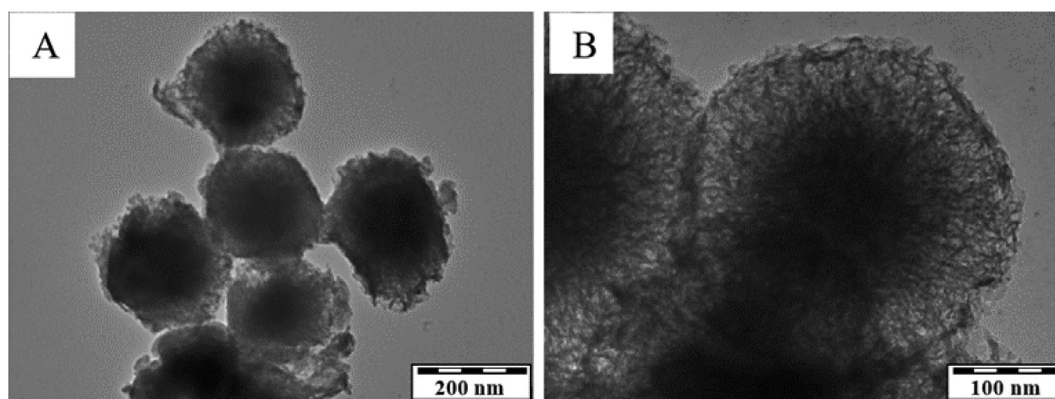


**Fig. 2.** TEM image of KCC-1 with different magnifications.

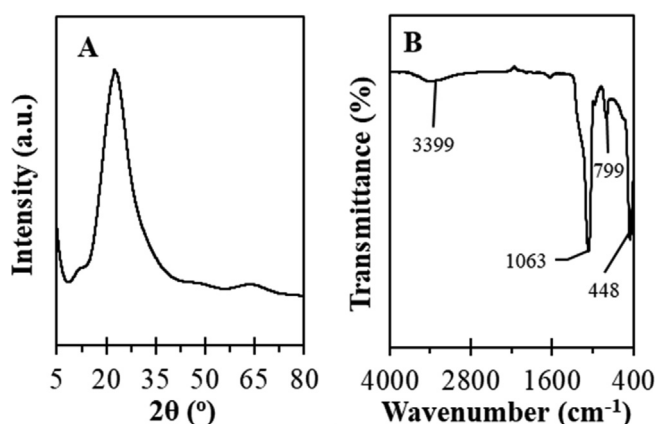


**Fig. 3.** (A) XRD pattern and (B) FTIR spectrum of KCC-1.

et al., 2016; Singh and Polshettiwar, 2016), indicating the successful synthesis of KCC-1.

### 3.2. Statistica analysis

The quadratic model of Pb(II) removal onto KCC-1 in term of coded forms is explicated by Eq. (3):

$$\begin{aligned}
 Y = & -18.8465 + 0.3102X_1 + 0.2469X_2 + 26.7658X_3 \\
 & - 0.0004X_1^2 + 0.0008X_2^2 - 2.6263X_3^2 - 0.0007X_1X_2 \\
 & - 0.0125X_1X_3 - 0.0460X_2X_3
 \end{aligned} \quad (3)$$

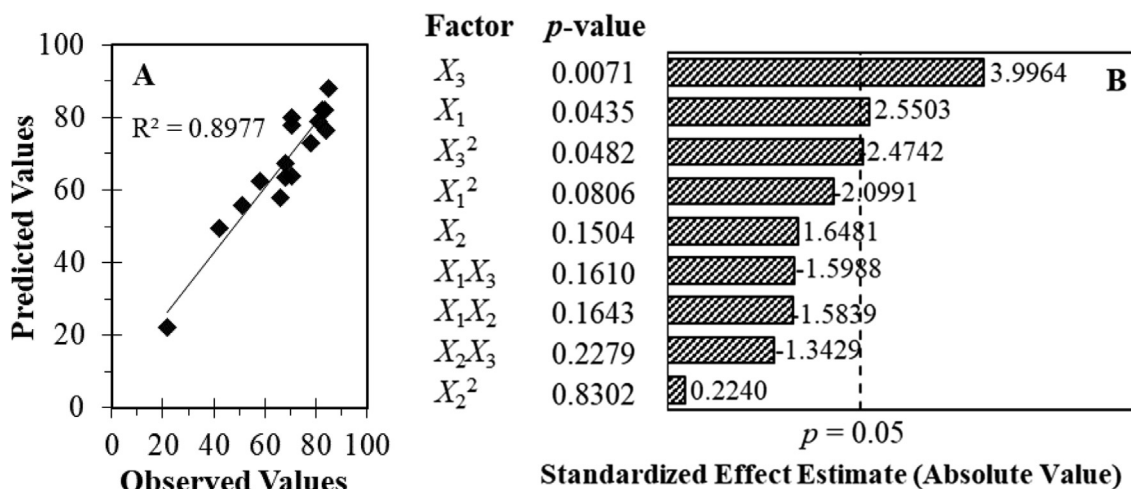
The adequacy and significance of the model were examined using ANOVA. By referring to the result observed in Table 2, the model was relatively significant as expressed by the greater calculated  $F$ -value ( $F_{model} = 5.85$ ) than that of the tabulated  $F$ -value ( $F_{table} = 4.10$ ) at 5% level of significance.

Fig. 4(A) shows the parity plot of the predicted and observed Pb(II) removal onto KCC-1 with the determination coefficient,  $R^2$  of 0.8977. In brief,  $R^2$  was used to test the correlation amidst predicted and experimental values whereby the value of  $R^2$  must be closed to 1.0 and should be at least 0.8 or greater for a good correlation of a model (Asfaram et al., 2015). Thus, high coefficient value of  $R^2$  portrayed that the model was successfully captured good correlation amidst the experimental and predicted values.

The Pareto chart and  $p$ -value for the Pb(II) removal onto KCC-1 are shown in Fig. 4(B). The significance of the factors can be examined by the  $p$ -value and  $t$ -value, whereby the corresponding factor with the greater magnitude of  $t$ -value ( $>2.4469$ ) and the smaller magnitude of  $p$ -value ( $<0.05$ ) portray as the more significant factor (Setiabudi et al., 2012). As demonstrated in Fig. 4(B), the linear term of initial concentration ( $X_1$ ), the linear term of adsorbent dosage ( $X_3$ ), and quadratic term of adsorbent dosage ( $X_3^2$ ) were sta-

**Table 2**  
ANOVA analysis of Pb(II) removal by KCC-1.

Sources	Sum of square (SS)	Degree of freedom ( <i>d,f</i> )	Mean Square (MS)	F-Value
Regression (SSR)	4007.33	9	445.26	5.85
Residual	456.75	6	76.13	
Total (SST)	4464.09	15		



**Fig. 4.** (A) Parity plot for the predicted and observed percentage of Pb(II) removal by KCC-1. (B) Pareto chart and *p*-value for Pb(II) removal by KCC-1.

tistically significant in this regression due to the large *t*-value magnitude and small *p*-value ( $p < 0.05$ ). The rest of the factor terms were considered less significant, due to a greater *p*-value ( $p > 0.05$ ). The linear term of adsorbent dosage ( $X_3$ ) was the most noteworthy factor for the regression model, while the quadratic term of time ( $X_2^2$ ) was the least noteworthy factor for the Pb(II) removal. The significant role of adsorbent dosage in Pb(II) removal might be due to the direct correlation of adsorbent dosage with the available number of binding sites for the Pb(II) interaction (Gyananath et al., 2012). In brief, an increase in quantity of adsorbent dosage simultaneously increase the number of available binding sites for the adsorption process. Similar results were also reported in the literature (Kahkha et al., 2014) for the Pb(II) adsorption onto Prosopis Stephanian Fruits. In their study, the influences of three independent factors (adsorbent dosage, pH, and initial concentration) were investigated, and the adsorbent dosage was found to be the most important factor.

Fig. 5(A) shows the simultaneous influences of initial concentration ( $X_1$ ) and time ( $X_2$ ) on Pb(II) removal. The percentage of Pb(II) removal increased with increment in initial Pb(II) concentration

and time until the optimal conditions ( $X_1 = 250$  mg/L–300 mg/L,  $X_2 = 70$ –90 min) was achieved, but slightly decreased at higher values. For the influence of the initial Pb(II) concentration, the increasing of initial Pb(II) concentration leads to an increase in driving force of Pb(II) ions onto the active sites of the KCC-1 and thus enhance the removal percentage (Kalantari et al., 2014). However, a decrement in removal percentage upon further increasing in Pb(II) concentration resulted from the saturation of the binding sites with adsorbed Pb(II) ions. For the influence of the time, the increase in Pb(II) removal at the beginning may be related to a high quantity of available binding sites on the surface of KCC-1, meanwhile, a slower adsorption rate at the final stage may be related to the decreasing of binding sites on the surface of KCC-1 (Ekka et al., 2015). Thus, the percentage of Pb(II) removal decreased after the optimum time achieved. Similar phenomenon on the influences of initial concentration and time towards Pb(II) removal was also reported by Kalantari et al. (2014) and Rajasimman and Murugaiyan (2012) using Fe<sub>3</sub>O<sub>4</sub>/Talc Nanocomposite and *Hypnea valentiae*, respectively.

Fig. 5(B) displays the simultaneous influences of time ( $X_2$ ) and adsorbent dosage ( $X_3$ ) on Pb(II) removal. As illustrated in the graph,

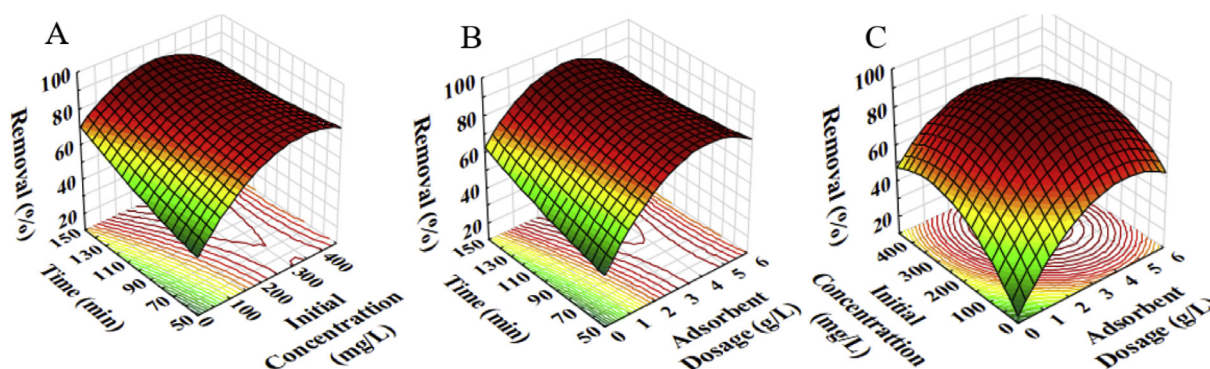


**Fig. 5.** The 3D surface plots showing the influences of (A) initial concentration ( $X_1$ ) and time ( $X_2$ ), (B) time ( $X_2$ ) and adsorbent dosage ( $X_3$ ), and (C) initial concentration ( $X_1$ ) and adsorbent dosage ( $X_3$ ).

the increase in time and adsorbent dosage resulted in an increase in Pb(II) removal, achieved the optimal ( $X_2 = 70\text{--}90$  min and  $X_3 = 3\text{--}4$  g/L), and slightly decreased at elevated adsorbent dosage. The positive role of adsorbent dosage in Pb(II) removal can be clarified by an increase in the available number of binding sites for the Pb(II) interaction (Rajasimman and Murugaiyan, 2012). The positive role of adsorbent dosage in heavy metal removal was also reported by Hamdzah et al. (2013) for the adsorption of Cu(II) and Pb(II) using straw/Fe<sub>3</sub>O<sub>4</sub> Nanocomposite.

Fig. 5(C) illustrates the simultaneous influences of initial concentration ( $X_1$ ) and adsorbent dosage ( $X_3$ ) on Pb(II) removal. The percentage of Pb(II) removal was improved with the increment in initial concentration and adsorbent dosage until it reached optimum at  $X_1 = 250\text{--}300$  mg/L and  $X_3 = 3\text{--}4$  g/L, and slightly decreased at higher values. In comparison with Fig. 5(A) and (B), it was clearly observed that the interaction of  $X_1X_3$  (Fig. 5(C)) significantly influence the Pb(II) removal as compared to the  $X_1X_2$  (Fig. 5(A)) and  $X_2X_3$  (Fig. 5(B)). This results in agreement with the lower  $p$ -value of factor  $X_1X_3$  as compared to the  $X_1X_2$  and  $X_2X_3$  (Fig. 4(B)). A noteworthy influence of initial concentration and adsorbent dosage on Pb(II) adsorption process was also reported by Asfaram et al. (2015) and Wang et al. (2017) for Pb(II) removal onto modified chitosan (MCMC-PEI) and modified activated carbon (Mn-Fe<sub>3</sub>O<sub>4</sub>-NPs-AC), respectively.

According to statistical study, the predicted Pb(II) removal was 84.54%, at  $X_1 = 281.7$  mg/L,  $X_2 = 3.7$  g/L, and  $X_3 = 80$  min. Additionally, three experiments were conducted at the predicted optimal conditions with the purpose to confirm the validity of the model. The average of three adsorption experiments was 83.06% of Pb(II) removal with the percentage error of 1.1%. The calculated Pb(II) adsorption capacity was 41.61 mg/g.

The performance of KCC-1 was compared with those of published works using various types of the adsorbent for Pb(II) removal as summarized in Table 3. It is clearly observed that the adsorption capacity of KCC-1 under the optimum condition is fairly high (41.61 mg/g) as compared to other types of mesoporous silica, which might due to the unique properties of KCC-1 with fibrous morphology and high surface area, indicating a great potential of KCC-1 to be used as an excellent adsorbent towards efficient removal of Pb(II).

### 3.3. Regeneration and reusability

The regeneration and reusability studies were applied at optimum condition predicted by RSM. For the regeneration study, the desorption process was executed using 0.1 M of nitric acid owing to its good performance in the treatment process as reported in the literature (Krukowska et al., 2017). As illustrated

**Table 3**  
Comparison of Pb(II) adsorption capacity of KCC-1 with several types of mesoporous silica adsorbent.

Adsorbent	Adsorption capacity (mg/g)	Ref
KCC-1	41.61	This study
Mesoporous silica	5.18	Ekka et al. (2015)
Bifunctional mesoporous silica spheres	7.15	Gomes et al. (2013)
Thiol-functionalized silica nano hollow sphere	17.15	Rostamian et al. (2011)
Silica functionalized with conjugated $\beta$ -ketoenol Furan	19.61	Radi et al. (2015)
MCM-41	34.33	Gang et al. (2015)
SBA-15-supported Pb(II)-imprinted polymer	38.01	Liu et al. (2011)

in Fig. 6, the performance of KCC-1 was declined by 33.38% with the increasing number of the cycles. This result might be due to the incomplete desorption of Pb(II) from the surface of KCC-1 (Lingamdinne et al., 2017) and thus resulted in the changes of the KCC-1's surface owing to the blockage of some available active sites by the Pb(II) (Vijayalakshmi et al., 2017). Although the adsorption performance of KCC-1 was slightly declined with the increasing number of cycles, however, the declined in removal percentage (33.38%, 5 cycles) of KCC-1 was lower than that of other reported adsorbents such as zeolite synthesized from low-calcium fly ash (48.84%, 2 cycles) (Ji et al., 2017), zeolite synthesized from high-calcium fly ash (62.79%, 2 cycles) (Ji et al., 2017), and modified potato starch-magnetic nanoparticles (MPS-MNPs) (50%, 4 cycles) (Abdul-Raheem et al., 2016). Additionally, the synthesized KCC-1 has high adsorption performance (83.06%) as compared to other silica structure such as Porphyrin modified SBA-15 (THPP-SBA-15) (80%) (Asgari et al., 2015) and APTES-mesoporous silica using chitosan as template (AMS) (67.98%) (Lalchhingpui et al., 2017), indicating high potential of KCC-1 as an adsorbent for Pb(II) removal.

Fig. 7 depicts the FTIR spectra, in the range of 4000–400 cm<sup>-1</sup>, for fresh KCC-1 (F1, F2, F3, F4, F5) (Fig. 7(A)) and spent KCC-1 (S1, S2, S3, S4, S5) (Fig. 7(B)) under five cycles of adsorbent reusability. The FTIR spectra of fresh KCC-1 exhibit adsorption peaks at 3399 cm<sup>-1</sup>, 1063 cm<sup>-1</sup>, 799 cm<sup>-1</sup>, and 448 cm<sup>-1</sup>, corresponding to O-H stretching vibration of Si-OH, the symmetrical stretching vibration of Si-O, the unsymmetrical stretching vibration of Si-O, and bending vibration of Si-O, respectively. After Pb(II) adsorption, all the mentioned peaks (3399 cm<sup>-1</sup>, 1063 cm<sup>-1</sup>, 799 cm<sup>-1</sup>, and 448 cm<sup>-1</sup>) were slightly shifted (3396 cm<sup>-1</sup>, 1062 cm<sup>-1</sup>, 800 cm<sup>-1</sup>, and 449 cm<sup>-1</sup>), which suggested the interaction of Pb(II) molecules with the functional groups of KCC-1. Additionally, owing to the important role of the negatively charged silanol group (Si-OH) in Pb(II) adsorption, the significant shifted of the peak at 3399 cm<sup>-1</sup> to 3396 cm<sup>-1</sup> may be related to the formation of Si-O-Pb upon the Pb(II) adsorption. The alteration of the FTIR peaks was also reported by Beh et al. (2012), indicating the participation of adsorbent's functional groups in metal binding process.

The presence of Pb(II) on the surface and pore of spent KCC-1 was further confirm by the N<sub>2</sub> physisorption analysis. It was found that the textural properties of KCC-1 ( $V_p = 0.3569$  m<sup>3</sup>/g and  $S_{BET} = 298.87$  m<sup>2</sup>/g) were significantly decreased after 5th cycle of

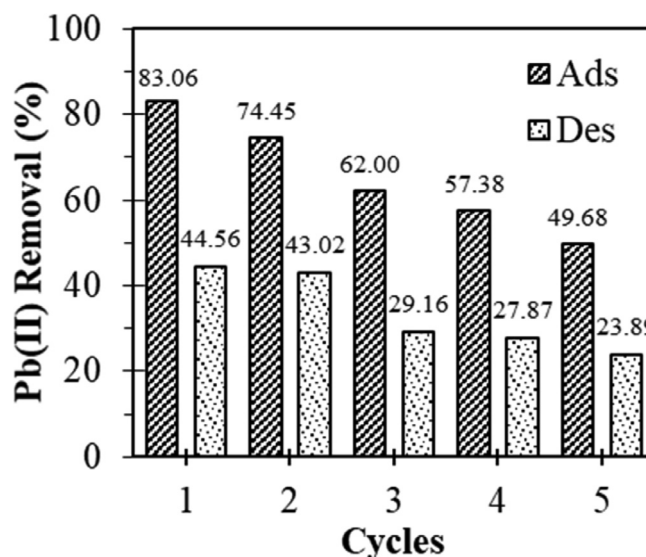


**Fig. 6.** Adsorption-desorption cycle of Pb(II) removal by KCC-1.

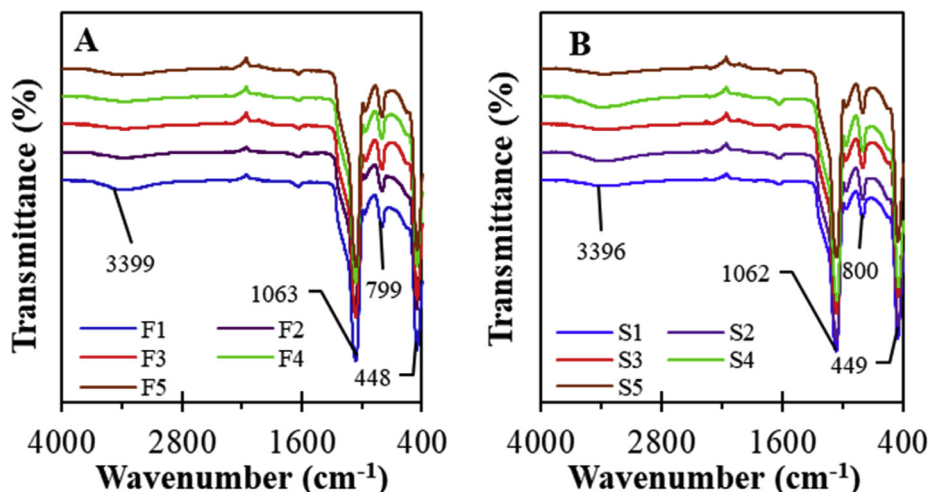


Fig. 7. FTIR spectra of (A) fresh KCC-1 (F1, F2, F3, F4, F5) and (B) spent KCC-1 (S1, S2, S3, S4, S5) under five cycles of adsorbent reusability.

adsorption process ( $V_p = 0.0824 \text{ m}^3/\text{g}$  and  $S_{\text{BET}} = 18.78 \text{ m}^2/\text{g}$ ), indicating the blockage of internal porosity of adsorbent by Pb(II) (Gedam and Dongre, 2015). A reduction in textural properties of adsorbent after adsorption process was also reported by Mirji et al. (2007) for SBA-15. They found that the  $V_p$  and  $S_{\text{BET}}$  of SBA-15 was decreased ( $V_p = 0.88 \text{ cm}^3/\text{g}$  to  $0.81 \text{ cm}^3/\text{g}$ ,  $S_{\text{BET}} = 387 \text{ m}^2/\text{g}$  to  $383 \text{ m}^2/\text{g}$ ) after the methanol adsorption indicating the blockage of pore with methanol molecules.

#### 4. Conclusion

In the present study, KCC-1 was successfully prepared and employed in the adsorption of Pb(II). The characterization of KCC-1 using TEM, XRD, FTIR, and BET proved that the KCC-1 contains fibrous silica structure with  $S_{\text{BET}} = 298.87 \text{ m}^2/\text{g}$ . The optimization of the independent factors (initial concentration ( $X_1$ ), time ( $X_2$ ), and adsorbent dosage ( $X_3$ )) on Pb(II) removal was executed using RSM combined with FCCCD. The optimal conditions were found at  $X_1 = 281.7 \text{ mg/L}$ ,  $X_2 = 80 \text{ min}$ , and  $X_3 = 3.7 \text{ g/L}$ , with Pb(II) removal of 84.54% predictably and 83.06% experimentally. The most significant factor was the linear term of adsorbent dosage ( $X_3$ ), while the quadratic term of time ( $X_2^2$ ) was the least significant factor. The feasibility of KCC-1 in Pb(II) removal was confirmed by its good performance during five cycles of reusability study. This study affirmed that the KCC-1 with fibrous morphology has a great potential to be used as an alternative adsorbent for Pb(II) removal with optimal Pb(II) removal of 83.06%.

#### Funding

This work was financially supported by Universiti Malaysia Pahang (UMP) through Research University Grant (RDU170331) and Postgraduate Research Grants Scheme (PGRS180305).

#### Conflict of interest

No known conflict of interest associated with this publication.

#### References

Abdul-Raheim, A.-R.M., Shama, M.E.-S., Reem, K., Manar, E.A.-R., 2016. Low cost biosorbents based on modified starch iron oxide nanocomposites for selective removal of some heavy metals from aqueous solutions. *Adv. Mat. Lett.* 7 (5), 402–409.

- Asfaram, A., Ghaedi, M., Goudarzi, A., Rajabi, M., 2015. Response surface methodology approach for optimization of simultaneous dye and metal ion ultrasound-assisted adsorption onto Mn doped  $\text{Fe}_3\text{O}_4$ -NPs loaded on AC: kinetic and isothermal studies. *Dalt. Trans.* 44, 14707–14723.
- Asgari, M.S., Zonouzi, A., Rahimi, R., Rabbani, M., 2015. Application of porphyrin modified sba-15 in adsorption of lead ions from aqueous media. *Orient. J. Chem.* 31 (3), 1537–1544.
- Baba, A.A., Adekola, F.A., 2013. Solvent extraction of Pb(II) and Zn(II) from a Nigerian galena ore leach liquor by tributylphosphate and bis(2,4,4-trimethylpentyl) phosphinic acid. *J. King Saud Univ. Sci.* 25 (4), 297–305.
- Beh, C.L., Chuah, T.G., Nourouzi, M.N., Choong, T.S.Y., 2012. Removal of heavy metals from steel making waste water by using electric arc furnace slag. *J. Chem.* 9, 2557–2564.
- Borah, L., Goswami, M., Phukan, P., 2015. Adsorption of methylene blue and eosin yellow using porous carbon prepared from tea waste: adsorption equilibrium, kinetics and thermodynamics study. *J. Environ. Chem. Eng.* 3, 1018–1028.
- Ekka, B., Rout, L., Kumar, M.K.S.A., Patel, R.K., Dash, P., 2015. Removal efficiency of Pb (II) from aqueous solution by 1-alkyl-3-methylimidazolium bromide ionic liquid mediated mesoporous silica. *J. Environ. Chem. Eng.* 3, 1356–1364.
- EPA, 2009. Environment Protection Agency. United States Environ. Prot. Agency. 816-F-09-004.
- Fatimah, I., 2018. Preparation, characterization and physicochemical study of 3-amino propyl trimethoxy silane-modified kaolinite for Pb(II) adsorption. *J. King Saud Univ. Sci.* 30 (2), 250–257.
- Gang, T.A.N., Yongjie, X.U.E., Jun, C.A.I., 2015. Isotherm study on adsorption removal of Pb(II) by MCM-41 zeolite synthesized from biomass ash. *Atl. Press. Iccset* 2014, 91–96.
- Gedam, A.H., Dongre, R.S., 2015. Adsorption characterization of Pb(ii) ions onto iodate doped chitosan composite: equilibrium and kinetic studies. *RSC Adv.* 5 (67), 54188–54201.
- Gomes, E.C.C., Sousa, A.F., Vasconcelos, P.H.M., Melo, D.Q., Diógenes, I.C.N., Sousa, E. H.S., Nascimento, R.F., Gil, R.A.S.S., Longhinotti, E., 2013. Synthesis of bifunctional mesoporous silica spheres as potential adsorbent for ions in solution. *Chem. Eng. J.* 214, 27–33.
- Gyananath, G., Balhal, D.K., Sciences, L., 2012. Removal of Lead (II) from aqueous solution by adsorption onto chitosan beads. *Cell Chem. Technol.* 46 (II), 121–124.
- Hamdaz, M., Ujang, Z., Nasef, M.M., Hadibarata, T., Olsson, G., Hassan, H., Rusli, M. M., 2013. Optimization of parameters affecting adsorption of Nickel (II), Zinc (II) and Lead (II) on dowex 50 W resin using a response surface methodology approach. *J. Environ. Sci. Technol.* 6, 106–118.
- Hamid, M.Y.S., Firmansyah, M.L., Triwahyono, S., Jalil, A.A., Mukti, R.R., Febriyanti, E., Suendo, V., Setiabudi, H.D., Mohamed, M., Nabgan, W., 2017. Oxygen vacancy-rich mesoporous silica KCC-1 for  $\text{CO}_2$  methanation. *App. Catal. A: Gen.* 532, 86–94.
- Hargreaves, A.J., Vale, P., Whelan, J., Alibardi, L., Constantino, C., Dotro, G., Cartmell, E., Campo, P., 2018. Impacts of coagulation-flocculation treatment on the size distribution and bioavailability of trace metals (Cu, Pb, Ni, Zn) in municipal wastewater. *Water Res.* 128, 120–128.
- Ji, X.D., Ma, Y.Y., Peng, S.H., Gong, Y.Y., Zhang, F., 2017. Simultaneous removal of aqueous  $\text{Zn}^{2+}$ ,  $\text{Cu}^{2+}$ ,  $\text{Cd}^{2+}$ , and  $\text{Pb}^{2+}$  by zeolites synthesized from low-calcium and high-calcium fly ash. *Wat. Sci. Technol.* 76 (8), 2106–2119.
- Kahkha, M.R.R., Piri, J., Kaykhaei, M., 2014. Application of response surface modeling and central composition design for removal of lead from aqueous solution using prosopis stephanian fruits. *Int. Res. J. Appl. Basic Sci.* 8, 701–706.
- Kalantari, K., Ahmad, M.B., Masoumi, H.R.F., Shamel, K., Basri, M., Khandanlou, R., 2014. Rapid adsorption of heavy metals by  $\text{Fe}_3\text{O}_4$ /talc nanocomposite and optimization study using response surface methodology. *Int. J. Mol. Sci.* 15, 12913–12927.

- Kelechi, E., Elvis, O.A., Kanayo, A.K., 2018. Synthesis and characterization of chitosan – silica hybrid aerogel using sol-gel method. *J. King Saud Univ. Sci.*, 1–5.
- Krukowska, J., Thomas, P., Kołodyn, D., 2017. Comparison of sorption and desorption studies of heavy metal ions from biochar and commercial active carbon. *Chem. Eng. J.* 307, 353–363.
- Lalchhingpuii, Tiwari, D., Lalhmunsiam, Lee, S.M., 2017. Chitosan templated synthesis of mesoporous silica and its application in the treatment of aqueous solutions contaminated with cadmium(II) and lead(II). *Chem. Eng. J.* 328, 434–444.
- Le, X., Dong, Z., Li, X., Zhang, W., Le, M., Ma, J., 2015. Fibrous nano-silica supported palladium nanoparticles: an efficient catalyst for the reduction of 4-nitrophenol and hydrodechlorination of 4-chlorophenol under mild conditions. *Catal. Commun.* 59, 21–25.
- Lingamdinne, L., Kim, I.-S., Ha, J.-H., Chang, Y.-Y., Koduru, J., Yang, J.-K., 2017. Enhanced adsorption removal of Pb(II) and Cr(III) by using nickel ferrite-reduced graphene oxide nanocomposite. *Metals (Basel)* 7, 225.
- Liu, Y., Liu, Z., Gao, J., Dai, J., Han, J., Wang, Y., Xie, Y.J., Yan, Y., 2011. Selective adsorption behavior of Pb(II) by mesoporous silica SBA-15-supported Pb(II)-imprinted polymer based on surface molecularly imprinting technique. *J. Hazard. Mater.* 186, 197–205.
- Lowe, B.M., Skylaris, C.K., Green, N.G., 2015. Acid-base dissociation mechanisms and energetics at the silica-water interface: an activationless process. *J. Colloid Interface Sci.* 451, 231–244.
- Merganpour, A.M., Nekuonam, G., Tomaj, O.A., Kor, Y., Safari, H., 2015. Efficiency of lead removal from drinking water using cationic resin Purolite. *Environ. Heal. Eng. Manag. J.* 2, 41–45.
- Mirji, S.A., Halligudi, S.B., Mathew, N., Jacob, N.E., Patil, K.R., Gaikwad, A.B., 2007. Adsorption of methanol on mesoporous SBA-15. *Mater. Lett.* 61 (1), 88–92.
- Okoye, C.C., Onukwuli, O.D., Okey-Onyesolu, C.F., 2018. Utilization of salt activated *Raphia hookeri* seeds as biosorbent for Erythrosine B dye removal: kinetics and thermodynamics studies. *J. King Saud Univ. Sci.*, 1–10.
- Ouyang, M., Wang, Y., Zhang, J., Zhao, Y., Wang, S., Ma, X., 2016. Three dimensional Ag/KCC-1 catalyst with a hierarchical fibrous framework for the hydrogenation of dimethyl oxalate. *RSC Adv.* 6, 12788–12791.
- Polshettiwar, V., Cha, D., Zhang, X., Basset, J.M., 2010. High-surface-area silica nanospheres (KCC-1) with a fibrous morphology. *Angew. Chem. Int. Ed.* 49, 9652–9656.
- Qureshi, Z.S., Sarawade, P.B., Hussain, I., Zhu, H., Johani, H.A., Anjum, D.H., Hedhili, M.N., Maity, N., D'Elia, V., Basset, J.-M., 2016. Gold nanoparticles supported on fibrous silica nanospheres (KCC-1) as efficient heterogeneous catalysts for CO oxidation. *ChemCatChem* 8, 1671–1678.
- Radi, S., Tighadouini, S., Massaoudi, M.E., Bacquet, M., Degoutin, S., Revel, B., Mabkhot, Y.N., 2015. Thermodynamics and kinetics of heavy metals adsorption on silica particles chemically modified by conjugated  $\beta$ -ketoenol furan. *J. Chem. Eng. Data* 60, 2915–2925.
- Rajasimman, M., Murugaiyan, K., 2012. Application of the statistical design for the sorption of lead by *hypnea valentiae*. *J. Adv. Chem. Eng.* 2, 1–7.
- Rengaraj, S., Yeon, K.-H., Moon, S.-H., 2001. Removal of chromium from water and wastewater by ion exchange resins. *J. Hazard. Mater.* 87, 273–287.
- Rostamian, R., Najafi, M., Rafati, A.A., 2011. Synthesis and characterization of thiol-functionalized silica nano hollow sphere as a novel adsorbent for removal of poisonous heavy metal ions from water: Kinetics, isotherms and error analysis. *Chem. Eng. J.* 171 (3), 1004–1011.
- Setiabudi, H.D., Jalil, A.A., Triwahyono, S., 2012. Ir/Pt-HZSM5 for n-pentane isomerization: Effect of iridium loading on the properties and catalytic activity. *J. Catal.* 294, 128–135.
- Siddiqui, S., 2015. DNA damage in Cicer plant grown on soil polluted with heavy metals. *J. King Saud Univ. Sci.* 27 (3), 217–223.
- Siddiqui, Z.N., Khan, K., Ahmed, N., 2014. Nano fibrous silica sulphuric acid as an efficient catalyst for the synthesis of  $\beta$ -enaminone. *Catal. Lett.* 144 (4), 623–632.
- Singh, B., Polshettiwar, V., 2016. Design of CO<sub>2</sub> sorbents using functionalized fibrous nanosilica (KCC-1): insights into the effect of the silica morphology (KCC-1 vs. MCM-41). *J. Mater. Chem. A* 4, 7071–7086.
- Tan, Y., Chen, M., Hao, Y., 2012. High efficient removal of Pb (II) by amino-functionalized Fe<sub>3</sub>O<sub>4</sub> magnetic nano-particles. *Chem. Eng. J.* 191, 104–111.
- Vijayalakshmi, K., Devi, B.M., Latha, S., Gomathi, T., Sudha, P.N., Venkatesan, J., Anil, S., 2017. Batch adsorption and desorption studies on the removal of lead (II) from aqueous solution using nanochitosan/sodium alginate/microcrystalline cellulose beads. *Int. J. Biol. Macromol.* 104, 1483–1494.
- Wang, Y., Wu, D., Wei, Q., Wei, D., Yan, T., Yan, L., Hu, L., Du, B., 2017. Rapid removal of Pb(II) from aqueous solution using branched polyethylenimine enhanced magnetic carboxymethyl chitosan optimized with response surface methodology. *Sci. Rep.* 7, 1–11.
- World Health Organization, 1984. Guidelines for Drinking Water Quality. World Heal. Organ., Geneva, Switzerland, pp. 1–2.
- Yousefzadeh, H., Salarian, A.A., Sid Kalal, H., 2018. Study of Pb (II) adsorption from aqueous solutions by TiO<sub>2</sub> functionalized with hydroxide ethyl aniline (PHEA/n-TiO<sub>2</sub>). *J. Mol. Liq.* 263, 294–302.